Dynamics and energy exchanges between a linear oscillator and a nonlinear absorber with local and global potentials

Simon Charlemagne, Claude-Henri Lamarque, Alireza Ture Savadkoohi

Dynamics and energy exchanges between a linear oscillator and a nonlinear absorber with local and global potentials

S. Charlemagne *, C.-H. Lamarque, A. Ture Savadkoohi

Univ Lyon, ENTPE, LGCB/LTDS UMR CNRS 5513, Rue Maurice Audin, F-69518 Vaulx-en-Velin Cedex, France

The dynamical behavior of a two degree-of-freedom system made up of a linear oscillator and a coupled nonlinear energy sink with nonlinear global and local potentials is studied. The nonlinear global potential of the energy sink performs direct interactions with the linear oscillator, while its local potential depends only on its own behavior during vibratory energy exchanges between two oscillators. A time multiple scale method around 1:1:1 resonance is used to detect slow invariant manifold of the system, its equilibrium and singular points. Detected equilibrium points permit us to predict periodic regime (s) while singular points can lead the system to strongly modulated responses characterized by persistent bifurcations. Several possible scenarios occurring during these strongly modulated regimes are highlighted. All analytical predictions are compared with those which are obtained by direct numerical integration of system equations.

1. Introduction

It has been demonstrated that nonlinear properties of oscillators can be used to localize vibratory energy of other coupled oscillators [1,2]. This idea was endowed to transfer, for a broad frequency range, vibratory energy of main structural systems to secondary coupled oscillators with very light masses compared to main ones' and with a nonlinear global potential function [3]. This phenomenon is named as energy pumping and the coupled light and nonlinear oscillator is called nonlinear energy sink (NES) [4,5]. Nonlinear absorbers used to mitigate vibrations such as nonlinear tuned vibration absorber (NLTVA) or nonlinear tuned mass damper (NLTMD) are studied in [6–8]. The NES can be applied to different varieties of engineering structures such as civil/mechanical [9–16], aerospace [17–19] and acoustical [20–22] engineering. McFarland et al. [9] and Kerschen et al. [10] investigate experimentally transient resonance capture in a system made of a linear oscillator and an ungrounded and grounded cubic NES, respectively. Gourdon et al. [11] deal with the design of a NES via analytical methods and its verifications with numerical simulations and experimental tests on a reduced-scale building. The control process of aeroelastic behavior of a theoretical two degree-of-freedom (dof) model of a bridge (with 2×2 Jordan block) coupled to a NES is studied in [12]. Vaurigaud et al. [13] prepare a theoretical design tool for control of a several dof system with several parallel NES at each dof. The same tools are endowed for designing two parallel NES at the last floor of a prototype building in [14]. Wierschem et al. [15] provide experimental results for a larger scale six-story structure coupled to a NES consisting of two light oscillators in series. Gourc et al. [16] study analytically and experimentally dynamical behavior of a linear oscillator and a coupled NES by formulating an optimization procedure for the passive control. Control of

* Corresponding author.
E-mail address: simon.charlemagne@entpe.fr (S. Charlemagne).

aeroelastic instability performed by a NES for applications in aerospace fields is studied analytically and experimentally in [17] and [18], respectively. The same problem is investigated by Luongo and Zulli [19] via a method mixing harmonic balance and multiple scale methods. In acoustics, the usage of nonlinear membranes as NES for passive control and energy pumping is explored by Cochelin et al. [20], Bellet et al. [21] and Shao and Cochelin [22].

However, in most of above-mentioned studies, the main structures are assumed to be linear or to present smooth nonlinearity [12,19] while the NES is supposed to have only a global cubic potential function, i.e. a cubic potential that interacts directly with the main oscillator. Other works are carried out to take into account other types of nonlinearities for the NES and/or to consider nonlinear main oscillators [23–37]. Shaw et al. [23] studied the response of a two-dof system consisting of a cubic oscillator and a cubic nonlinear absorber, particularly quasi-periodic responses. A similar system with nonlinear damping is investigated by Zhu et al. [24]. Energy exchanges between a main linear oscillator and a non-polynomial and nonsmooth NES are studied by Gendelman [25] and Lamarque et al. [26], respectively. The latter system in the presence of the gravity is studied by Ture Savadkoohi et al. [27]. Nucera et al. [28] experimentally traced the passive control process between a linear system and a coupled vibro-impact NES. More, theoretical and experimental developments of control process of system by vibro-impact NES are achieved by Gendelman [29] and Gourc et al. [30]. Recently, Gendelman and Alloni [31] developed a technique for tracing chaotic strongly modulated regimes during passive control by vibro-impact NES. Energy transfer from a main linear structure with varying mass to a nonsmooth NES is studied in [32]. Besides, energy exchanges between main oscillators with nonlinear or nonsmooth rheologies and smooth or nonsmooth NES devices have been studied. Passive control of nonsmooth and Dahl type main structures coupled to nonsmooth NES is studied in [33,34], respectively. Vibratory energy exchanges between a main oscillator with a single or a set of Saint-Venant elements and a cubic NES is studied in [35,36]. Passive control of main structural systems with hysteresis behavior by nonsmooth NES is studied in [37].

In this paper, the behavior of two coupled oscillator is studied: the main structure, which is supposed to be linear, is coupled to a NES with local and global potential functions, both nonlinear, which is new. A few works, some among the above-cited references, study secondary oscillator with a linear global potential and a nonlinear local one [10,20–22,36,38–41], i.e. a potential that depends only on the response of the NES. Some of them consider a NES whose mass must be of the same order as the main system's one to perform passive control [10,20,36,38,39]. Malatkar and Nayfeh [40] investigate the same system as Jiang et al. [38] using different methods (harmonic balance method, a combination of a shooting method and Floquet theory, and direct time integration), without finding any evidence of energy pumping. A new method based on comparing backbone curves and forced responses has also been recently suggested and applied to a two-dof system with two nonlinearly coupled cubic forced oscillators by Hill et al. [41]. Bellet et al. [21] and Shao and Cochelin [22] show evidence of energy pumping in an acoustic cavity linearly coupled to a membrane presenting cubic local nonlinearity and nonlinear damping. In this study, we choose a given form of local potential and we try to highlight its effects on the behavior of the system at different regimes in comparison of a system including only a nonlinear global potential. Local potential can occur for instance due to contact between structural elements during the excitation, or be intentionally realized for enhancing efficiencies of NES devices for passive control and/or energy harvesting purposes. Organization of the paper is as follows: the mathematical model of the overall system, change of variables, complexification and keeping first harmonics by truncating higher order ones are explained in Section 2. The system behavior at fast time scale by detecting its invariant manifold and stability zones is discussed in Section 3. The dynamics of the system at slow time scale by tracing its equilibrium and singular points, corresponding to periodic and strongly modulated regimes respectively, are studied in Section 4. Existence of some possible scenarios during energy exchanges between the two oscillators is illustrated in Section 5. Finally the paper is concluded in Section 6.

2. Model description

Let us consider the two dof system which is depicted in Fig. 1. The principal structure is supposed to be linear and to have the mass M, the damping $\hat{a}$ and the stiffness K. It is subjected to the external force $F(t)$. The main system is coupled to a NES with the very light mass m and the damping $\hat{c}$. The NES possesses two types of potentials: the global one, $\tilde{V}$, which consists

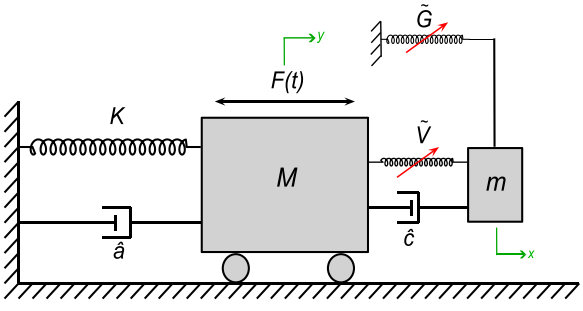

Fig. 1. The two dof system made up of a linear structure under external excitation $F(t)$ coupled to a nonlinear oscillator ($m = \epsilon M$, $0 < \epsilon \ll 1$).

of linear and nonlinear parts and the local nonlinear one, $\tilde{G}$, which is only connected to the mass m. The mass ratio of the two oscillators, i.e. ϵ, is very small:

$$0 < \epsilon = \frac{m}{M} \ll 1 \tag{1}$$

Let us assume that x and y stand for displacements of the NES and the principal structure, respectively. Governing equations of the described system can be summarized as:

$$\begin{cases} M\ddot{y} + \hat{a}\dot{y} + Ky + \hat{c}(\dot{y}-\dot{x}) + \tilde{V}(y-x) = F(t) \\ m\ddot{x} + \hat{c}(\dot{x}-\dot{y}) + \tilde{V}(x-y) + \tilde{G}(x) = 0 \end{cases} \tag{2}$$

or

$$\begin{cases} \ddot{y} + a\dot{y} + \omega_0^2 y + c(\dot{y}-\dot{x}) + \omega_c^2(y-x) + W(y-x) = f(t) \\ \epsilon\ddot{x} - c(\dot{y}-\dot{x}) - \omega_c^2(y-x) - W(y-x) + \tilde{g}(x) = 0 \end{cases} \tag{3}$$

where $\frac{\hat{a}}{M} = a$, $\frac{K}{M} = \omega_0^2$, $\frac{\hat{c}}{M} = c$, $\frac{\tilde{V}(y-x)}{M} = \omega_c^2(y-x) + W(y-x)$, $\frac{F(t)}{M} = f(t)$, $\frac{\tilde{G}(x)}{M} = \tilde{g}(x)$. It can be seen that the global potential $\tilde{V}(y-x)$ of the NES is sum of linear ($\omega_c^2(y-x)$) and nonlinear ($W(y-x)$) parts. Both nonlinear potentials of the NES are assumed to be odd functions. Their expressions will be given later in order to keep a general form of the equations as long as possible. We introduce the displacement of the center of masses v and the relative displacement w as new variables of the system:

$$\begin{cases} v = \frac{y+\epsilon x}{1+\epsilon} \\ w = x - y \end{cases} \Leftrightarrow \begin{cases} y = v - \frac{\epsilon}{1+\epsilon} w \\ x = v + \frac{1}{1+\epsilon} w \end{cases} \tag{4}$$

Eq. (3) reads as:

$$\begin{cases} (1+\epsilon)\ddot{v} + a\left(\dot{v} - \frac{\epsilon}{1+\epsilon}\dot{w}\right) + \omega_0^2\left(v - \frac{\epsilon}{1+\epsilon}w\right) + \tilde{g}\left(v + \frac{1}{1+\epsilon}w\right) = f(t) \\ \ddot{w} - a\left(\dot{v} - \frac{\epsilon}{1+\epsilon}\dot{w}\right) - \omega_0^2\left(v - \frac{\epsilon}{1+\epsilon}w\right) + \frac{1+\epsilon}{\epsilon}\left(c\dot{w} + \omega_c^2 w + W(w)\right) + \frac{1}{\epsilon}\tilde{g}\left(v + \frac{1}{1+\epsilon}w\right) = -f(t) \end{cases} \tag{5}$$

Following complex variables of Manevitch [42] are introduced to Eq. (5):

$$\begin{cases} \psi e^{i\omega t} = \dot{v} + i\omega v \\ \varphi e^{i\omega t} = \dot{w} + i\omega w \end{cases} \tag{6}$$

with $i^2 = -1$ and ω is the frequency of the external force which will be introduced later on. In order to deal with nonlinear system equations, we will endow a multiple scale method [43] by embedding the time to fast and slow scales which are connected to each other by the mass ratio of the two oscillators, i.e. ϵ. New scales of time read as: $\tau_j = \epsilon^j t, j = 0, 1, \ldots$ where τ_0 is the fast time scale and τ_1, τ_2, etc. are slow time scales. Introducing $D_j = \frac{d}{d\tau_j}$, one can write:

$$\frac{d}{dt} = D_0 + \epsilon D_1 + \epsilon^2 D_2 + \cdots \tag{7}$$

Following assumptions are made:

- The forcing amplitude is at the ϵ^1 order, oscillating with the pulsation ω: $f(t) = \epsilon f^0 \sin(\omega t)$.
- We investigate the system behavior around 1:1:1 resonance: $\omega = \omega_0(1+\sigma\epsilon)$.
- Damping coefficients are small and at the order of ϵ^1: $c = \epsilon d$ and $a = \epsilon a_0$.
- Linear part of the global potential is at the ϵ^1 order: $\omega_c^2 = \epsilon\Omega^2$.
- Nonlinear parts of potentials of the NES are at the ϵ^1 order: $\tilde{g}(x) = \epsilon\tilde{g}^0(x)$ and $W(y-x) = \epsilon W^0(y-x)$.

We implement the Galerkin technique by keeping first harmonics and truncating higher order ones. This task is carried out for an arbitrary function s by imposing following integral:

$$S = \frac{\omega}{2\pi}\int_0^{\frac{2\pi}{\omega}} s(\tau_0) e^{-i\omega\tau_0}\, d\tau_0 \tag{8}$$

We assume that ψ and φ do not depend on τ_0. We will either verify this assumption during the multiple scale analysis or we will assume that after a transient regime long enough, ψ and φ reach an asymptotic state which is independent of the time τ_0. Nevertheless, we also keep $\dot{\psi}$ and $\dot{\varphi}$ in the equations because of their dependence on multiple time scales. After applying complex variables of Manevitch, which are given in Eqs. (6), to Eq. (5) and using the Galerkin technique (Eq. (8)), following

system of equations can be obtained:

$$\begin{cases} \dot{\psi}+\left(\frac{\mathrm{i}\omega_0(1+\sigma\epsilon)}{2}+\frac{a_0\epsilon}{2(1+\epsilon)}-\frac{\mathrm{i}\omega_0}{2(1+\epsilon)(1+\sigma\epsilon)}\right)\psi-\frac{\epsilon}{2(1+\epsilon)^2}\left(a_0\epsilon-\frac{\mathrm{i}\omega_0}{1+\sigma\epsilon}\right)\varphi+\frac{\epsilon}{1+\epsilon}F_{\tilde{g}^0}=-\frac{\epsilon}{1+\epsilon}\frac{\mathrm{i}f^0}{2} \\ \dot{\varphi}+\left(\frac{\mathrm{i}\omega_0(1+\sigma\epsilon)}{2}+\frac{a_0\epsilon^2}{2(1+\epsilon)}-\frac{\mathrm{i}\omega_0\epsilon}{2(1+\epsilon)(1+\sigma\epsilon)}+\frac{d(1+\epsilon)}{2}-\frac{\mathrm{i}\Omega^2(1+\epsilon)}{2\omega_0(1+\sigma\epsilon)}\right)\varphi-\left(\frac{a_0\epsilon}{2}-\frac{\mathrm{i}\omega_0}{2(1+\sigma\epsilon)}\right)\psi+(1+\epsilon)F_{W^0}+F_{\tilde{g}^0}=\epsilon\frac{\mathrm{i}f^0}{2} \end{cases} \tag{9}$$

where

$$\begin{cases} F_{\tilde{g}^0}=\frac{\omega}{2\pi}\int_0^{\frac{2\pi}{\omega}}\tilde{g}^0\left(\frac{\psi e^{\mathrm{i}\omega t}-\psi^* e^{-\mathrm{i}\omega t}}{2\mathrm{i}\omega}+\frac{1}{1+\epsilon}\frac{\varphi e^{\mathrm{i}\omega t}-\varphi^* e^{-\mathrm{i}\omega t}}{2\mathrm{i}\omega}\right)e^{-\mathrm{i}\omega t}\,\mathrm{d}t \\ F_{W^0}=\frac{\omega}{2\pi}\int_0^{\frac{2\pi}{\omega}}W^0\left(\frac{\varphi e^{\mathrm{i}\omega t}-\varphi^* e^{-\mathrm{i}\omega t}}{2\mathrm{i}\omega}\right)e^{-\mathrm{i}\omega t}\,\mathrm{d}t \end{cases} \tag{10}$$

3. The system behavior at ϵ^0 order: fast time scale

3.1. The slow invariant manifold of the system

Studying Eq. (9) at fast time scale is equivalent to analyzing the system of equations at ϵ^0 order, which reads:

$$\begin{cases} D_0\psi=0\Rightarrow\psi=\psi(\tau_1,\tau_2,\ldots) \\ D_0\varphi+\left(\frac{\mathrm{i}\omega_0}{2}+\frac{d}{2}-\frac{\mathrm{i}\Omega^2}{2\omega_0}\right)\varphi+\frac{\mathrm{i}\omega_0}{2}\psi+F_{W^0}+F_{\tilde{g}^0}=0 \end{cases} \tag{11}$$

We assume that local potential and nonlinear part of global potential of the NES are cubic functions as it follows:

$$\begin{cases} W^0(y-x)=\mathcal{A}^0(y-x)^3 \\ \tilde{g}^0(x)=\mathcal{B}^0x^3 \end{cases} \tag{12}$$

Cubic potential functions are chosen for the following reasons: they are widely used in the literature and a cubic potential is convenient for possible experimental studies since it can be realized thanks to two linear springs [11]. Nonetheless, the analytical method used in this study can be applied to different types of nonlinearities, as shown in [25,26] where the NES has nonsmooth and non-polynomial nonlinearities, respectively. Fixed points of Eq. (11) at the ϵ^0 order (i.e. ϕ) satisfy:

$$\lim_{\tau_0\to+\infty}D_0\varphi=0 \tag{13}$$

Then slow invariant manifold (SIM) of the system can be defined as:

$$\left(\frac{\mathrm{i}\omega_0}{2}+\frac{d}{2}-\frac{\mathrm{i}\Omega^2}{2\omega_0}\right)\phi+\frac{\mathrm{i}\omega_0}{2}\psi-\mathrm{i}\mathcal{A}|\phi|^2\phi-\mathrm{i}\mathcal{B}|\psi+\phi|^2(\psi+\phi)=0 \tag{14}$$

where

$$\begin{cases} \mathcal{A}=\frac{3\mathcal{A}^0}{8\omega_0^3} \\ \mathcal{B}=\frac{3\mathcal{B}^0}{8\omega_0^3} \end{cases} \tag{15}$$

Let us introduce the variable χ as:

$$\chi=\psi+\phi \tag{16}$$

Eq. (14) reads:

$$\left(\frac{\mathrm{i}\omega_0}{2}\chi+\quad d-\frac{\mathrm{i}\Omega^2}{\omega_0}\right)\frac{\phi}{2}-\mathrm{i}\mathcal{A}|\phi|^2\phi-\mathrm{i}\mathcal{B}|\chi|^2\chi=0 \tag{17}$$

Writing the variables in terms of polar coordinates:

$$\begin{cases} \chi=\rho e^{\mathrm{i}\theta} \\ \psi=N_1e^{\mathrm{i}\delta_1} \\ \phi=N_2e^{\mathrm{i}\delta_2} \end{cases} \tag{18}$$

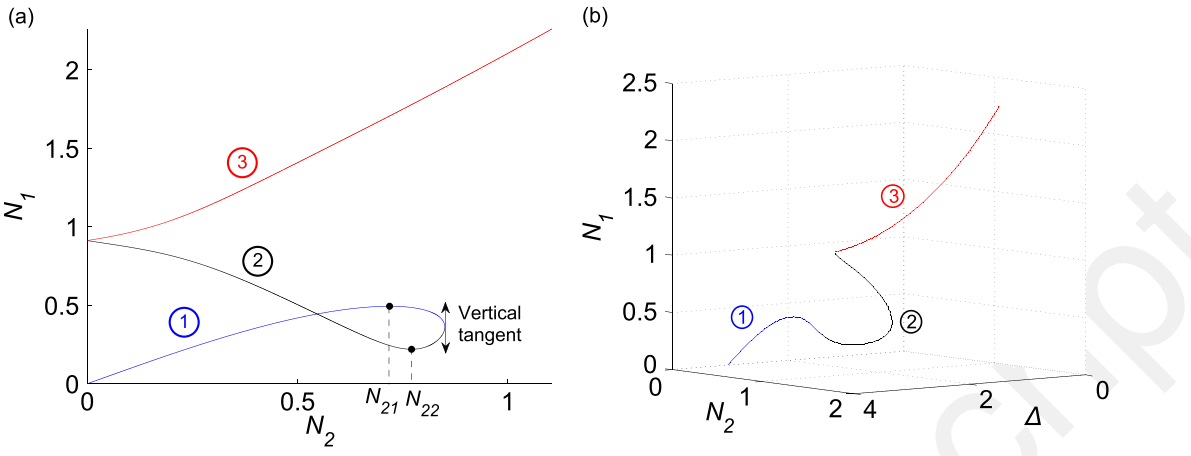

Fig. 2. (a) Two dimensional flow of the SIM of the system in the (N_2, N_1) plane – (b) Three dimensional flow of the SIM of the system in the (Δ, N_2, N_1) space – $\mathcal{A}=0.25$, $\mathcal{B}=0.6$, $d=0.1$, $\omega_0=1$ and $\Omega=0.2$.

and after separation of real and imaginary parts of Eq. (17), we obtain:

$$\begin{cases} \rho\ \cos\ (\Theta) = \dfrac{\dfrac{\Omega^2}{2\omega_0} + \mathcal{A}N_2^2}{\dfrac{\omega_0}{2} - \mathcal{B}\rho^2} N_2 \\ \rho\ \sin\ (\Theta) = \dfrac{d}{\omega_0 - 2\mathcal{B}\rho^2} N_2 \end{cases} \tag{19}$$

with $\Theta = \theta - \delta_2$. Following equation can be obtained:

$$\left(\frac{\omega_0}{2} - \mathcal{B}\rho^2\right)^2 \rho^2 - \left(\frac{d^2}{4} + \frac{\Omega^2}{2\omega_0} + \mathcal{A}N_2^2\right)^2 N_2^2 = 0 \tag{20}$$

Eq. (20) is a polynomial of degree three which can be solved by Cardano's method. Since ρ is an amplitude ($\chi = \rho e^{i\theta}$), it should be real positive number. Depending on N_2, there are one, two or three real expressions of ρ. Then, from Eqs. (16) and (18), a polynomial equation of N_1 can be obtained versus N_2. This means that SIM of the system in the form of amplitudes N_2 and N_1 can be traced.

3.2. An example for SIM

As an example, let us assume that $\mathcal{A}=0.25$, $\mathcal{B}=0.6$, $d=0.1$, $\omega_0=1$ and $\Omega=0.2$. The corresponding SIM of such a system is illustrated in Fig. 2(a). It possesses three branches, i.e. three possible values of N_1 for each N_2, corresponding to the three real solutions of ρ in Eq. (20). Branches ① and ② of the SIM possess local maximum and minimum, respectively. By comparison, invariant manifold of such coupled systems without local potential also possesses two local extrema. Moreover, in traditional SIM, there is only one value of N_1 for each N_2 [16] whereas the presented SIM in this work gives multiplicity of solutions. Energy of the NES N_2 at local maximum and minimum is named as N_{21} and N_{22}, respectively. Note that both of these two extrema can be located on branch ① for different shapes of the SIM which will be presented later on. Branch ② has an intersection with N_1-axis at the point $\left(0, \sqrt{\frac{\omega_0}{2\mathcal{B}}}\right)$ which is the start point for branch ③. One can see that the limit case $\mathcal{B}=0$ (i.e. absence of the local potential) cannot be considered directly. The intersection of branches ① and ② is a point where the tangent of the SIM is vertical and "could" lead to a possible vertical jump towards branch ③. This will be verified in detail in Section 4.

Moreover, branches ① and ② of the SIM "seem" to cross each other. The three dimensional view of the invariant, i.e. in $(\Delta = \delta_1 - \delta_2, N_2, N_1)$ space, will help us to enlighten this illusion. Let us introduce $C = \omega_0 - \frac{\Omega^2}{\omega_0}$ in Eq. (14) and separate its real $(\mathcal{F}_1)$ and imaginary $(\mathcal{F}_2)$ parts:

$$\begin{cases} \mathcal{F}_1 = \dfrac{d}{2}N_2 - \dfrac{\omega_0}{2}N_1\ \sin(\Delta) + \mathcal{B}\left(N_1^2 + N_2^2 + 2N_1N_2\ \cos(\Delta)\right)N_1 \sin(\Delta) = 0 \\ \mathcal{F}_2 = \dfrac{C}{2}N_2 + \dfrac{\omega_0}{2}N_1\ \cos(\Delta) - \mathcal{A}N_2^3 - \mathcal{B}\left(N_1^2 + N_2^2 + 2N_1N_2\ \cos(\Delta)\right)(N_2 + N_1\cos(\Delta)) = 0 \end{cases} \tag{21}$$

These equations can be solved for tracing the three dimensional flow of the SIM. The three dimensional form of the presented SIM in Fig. 2(a) is depicted in Fig. 2(b). It can be seen that due to different phases, branches ① and ② of the SIM do

not cross each other. Thus, projection of the SIM in the plane (N_1, N_2) is not sufficient to interpret the behavior of a system with local potential.

3.3. Stable and unstable zones of the SIM

In order to highlight unstable zones of the SIM, we introduce infinitesimal perturbation of φ in the second equation of Eq. (11) as:

$$\varphi \to \varphi + \Delta\varphi, \quad |\Delta\varphi| \ll |\varphi| \tag{22}$$

ψ is not perturbed since it is independent of τ_0 (see Eq. (11)). The linearized form of the equation obtained by keeping only the first orders of $\Delta\varphi$ and its conjugate read:

$$\begin{pmatrix} \frac{\partial \Delta\varphi}{\partial \tau_0} \\ \frac{\partial \Delta\varphi^*}{\partial \tau_0} \end{pmatrix} = \underbrace{\begin{pmatrix} M_1 & M_2 \\ M_2^* & M_1^* \end{pmatrix}}_{\boldsymbol{M}} \begin{pmatrix} \Delta\varphi \\ \Delta\varphi^* \end{pmatrix} \tag{23}$$

with

$$\begin{cases} M_1 = -\left(\frac{d}{2} + \mathrm{i}\frac{C}{2}\right) + 2\mathrm{i}\,\mathcal{A}|\varphi|^2 + 2\mathrm{i}\mathcal{B}\left(|\psi|^2 + |\varphi|^2 + \psi\varphi^* + \varphi\psi^*\right) \\ M_2 = \mathrm{i}\mathcal{A}\varphi^2 + \mathrm{i}\mathcal{B}(\psi^2 + \varphi^2 + 2\psi\varphi) \end{cases} \tag{24}$$

where $(\cdot)^*$ stands for the complex conjugate. Here, the sign of the real part of the eigenvalues of matrix $\boldsymbol{M}$ will localize possible unstable zones of the SIM. Indeed, if at least one of its eigenvalues has a positive real part, $\Delta\varphi$ will exponentially diverge versus time, creating instability around the SIM. The characteristic equation of the matrix $\boldsymbol{M}$ reads:

$$P_{car}(X) = X^2 - (M_1 + M_1^*)X + |M_1|^2 - |M_2|^2 \tag{25}$$

The sum and product of the eigenvalues are $M_1 + M_1^* = -d < 0$ and $|M_1|^2 - |M_2|^2$, respectively. Thus, the system will be unstable if $|M_1|^2 - |M_2|^2 < 0$. Unstable zones of the SIM are actually encased between local extrema.

4. The system behavior at ϵ^1 order: slow time scale

Let us consider the first equation of Eq. (9) at the ϵ^1 order:

$$D_1\psi + \left(\mathrm{i}\omega_0\left(\sigma + \frac{1}{2}\right) + \frac{a_0}{2}\right)\psi + \frac{\mathrm{i}\omega_0}{2}\varphi - \mathrm{i}\mathcal{B}|\psi + \varphi|^2(\psi + \varphi) = -\frac{\mathrm{i}f^0}{2} \tag{26}$$

This equation gives us necessary tools for detecting equilibrium points and fold singularities of the system at τ_1 time scale.

4.1. Equilibrium points of the system

We are interested in searching for equilibrium points of the system at slow time scale around its SIM. The equilibrium points correspond to periodic regimes (stable or unstable) with different possible situations for the energy of the main oscillator and the NES. Let us set:

$$D_1\psi = 0 \tag{27}$$

Eq. (26) reads:

$$\left(\mathrm{i}\omega_0\left(\sigma + \frac{1}{2}\right) + \frac{a_0}{2}\right)\psi + \frac{\mathrm{i}\omega_0}{2}\varphi - \mathrm{i}\mathcal{B}|\psi + \varphi|^2(\psi + \varphi) = -\frac{\mathrm{i}f^0}{2} \tag{28}$$

We are interested in analyzing system behaviors around the SIM. Subtracting Eq. (28) from Eq. (14) which is obtained at the infinity of τ_0 time scale (see Eq. (13)), one can obtain:

$$N_1 e^{\mathrm{i}\Delta} = \frac{\beta N_2 - \mathrm{i}\frac{f^0}{2}e^{-\mathrm{i}\delta_2}}{\alpha} \tag{29}$$

with

$$\begin{cases} \alpha = \mathrm{i}\omega_0\sigma + \frac{a_0}{2} \\ \beta = \frac{d + \mathrm{i}(C - \omega_0)}{2} - \mathrm{i}\mathcal{A}N_2^2 \end{cases} \tag{30}$$

Moreover, the SIM (Eq. (14)) can be reformulated as:

$$\frac{d+\mathrm{i}C}{2}N_2-\mathrm{i}\mathcal{A}N_2^3+\frac{\mathrm{i}\omega_0}{2}N_1e^{\mathrm{i}\Delta}-\mathrm{i}\mathcal{B}\rho^2\left[N_2+N_1e^{\mathrm{i}\Delta}\right]=0 \tag{31}$$

Eq. (31) is a function of ρ. As seen in Section 3.1, existence of multiple solutions of ρ defines three branches of the SIM. As a consequence, depending on the investigated branch, there will be different expressions of Eq. (31). By injecting Eq. (29) into Eq. (31), real (H_1) and imaginary (H_2) parts of the obtained system read:

$$\begin{cases} H_1=\left(\beta_r-\mu_i\left(\frac{\omega_0}{2}-\mathcal{B}\rho^2\right)\right)N_2+\frac{f^0}{2}\left(\frac{\omega_0}{2}-\mathcal{B}\rho^2\right)\left(\eta_r\ \cos\left(\delta_2\right)+\eta_i\ \sin\left(\delta_2\right)\right)=0 \\ H_2=\left(\beta_i+\left(1+\mu_r\right)\left(\frac{\omega_0}{2}-\mathcal{B}\rho^2\right)\right)N_2+\frac{f^0}{2}\left(\frac{\omega_0}{2}-\mathcal{B}\rho^2\right)\left(\eta_i\ \cos\left(\delta_2\right)-\eta_r\ \sin\left(\delta_2\right)\right)=0 \end{cases} \tag{32}$$

where β_r, β_i, μ_r, μ_i, η_r and η_i are functions of the parameters and N_2 whose expressions are given in Appendix A. Thus, each pair (N_2,δ_2) that satisfies $H_{1j}=H_{2j}=0$ is an equilibrium point, where H_{1j} and H_{2j} are the expressions of H_1 and H_2 on the j^{th} branch.

4.2. Singular points of the system

Let us consider Eq. (21). Evolutions of the SIM at τ_1 time scale read:

$$\frac{d\mathcal{F}_j}{d\tau_1}=0,\quad j=1,2 \tag{33}$$

which in the matrix form can be rewritten as:

$$\underbrace{\begin{pmatrix}\frac{\partial\mathcal{F}_1}{\partial N_2} & \frac{\partial\mathcal{F}_1}{\partial\Delta}\\ \frac{\partial\mathcal{F}_2}{\partial N_2} & \frac{\partial\mathcal{F}_2}{\partial\Delta}\end{pmatrix}}_{\boldsymbol{D}}\begin{pmatrix}\frac{dN_2}{d\tau_1}\\ \frac{d\Delta}{d\tau_1}\end{pmatrix}=-\begin{pmatrix}\frac{\partial\mathcal{F}_1}{\partial N_1}\\ \frac{\partial\mathcal{F}_2}{\partial N_1}\end{pmatrix}\frac{dN_1}{d\tau_1} \tag{34}$$

The expression of $\frac{dN_1}{d\tau_1}$ is known from Eq. (26). Singular points of the system (34) can be detected by setting the determinant of the matrix $\boldsymbol{D}$ to zero. As a summary following criteria provide positions of fold singularities of the system at τ_1 time scale around the SIM:

$$\begin{cases}\mathcal{F}_1=0\\ \mathcal{F}_2=0\\ \det(D)=0\end{cases} \tag{35}$$

and

$$\begin{cases}H_1=0\\ H_2=0\end{cases} \tag{36}$$

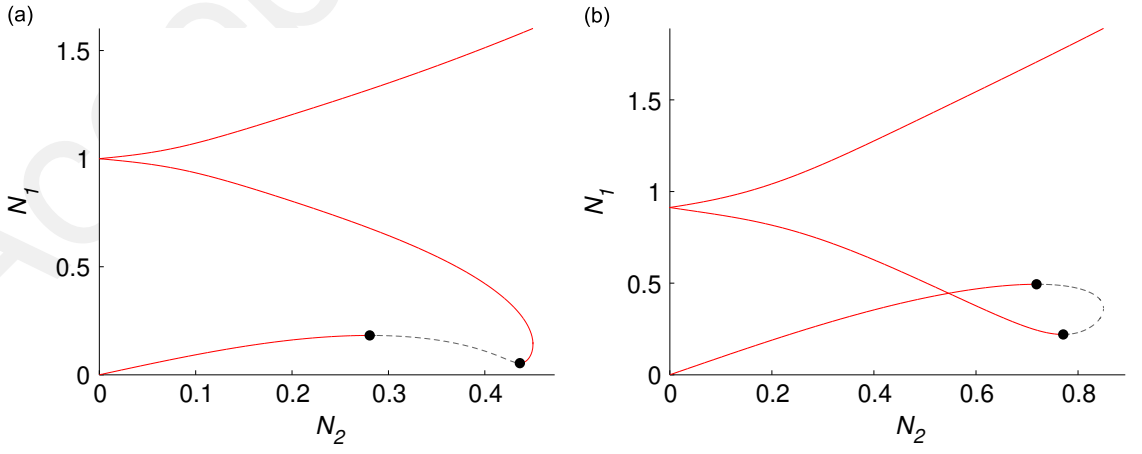

Fig. 3. Positions of the two singular points of the system on the SIM – (a) $d=0.1$, $\omega_0=1$, $\Omega=0.2$, $\mathcal{A}=2$ and $\mathcal{B}=0.5$ – (b) $d=0.1$, $\omega_0=1$, $\Omega=0.2$, $\mathcal{A}=0.25$ and $\mathcal{B}=0.6$ – unstable zones are plotted in gray dotted lines.

Fig. 3 summarizes positions of singular points verifying system (35) with two given sets of parameters. Unstable zones of the SIM are plotted in dotted lines. If the system, in addition to system (35), verifies system (36) as well, which depends on external forcing term and the de-tuning parameter (σ), then the system possesses fold singularities. In this case, equilibrium and singular points coincide. It can be seen that local maximum ($N_2 = N_{21}$) and minimum ($N_2 = N_{22}$) match conditions of singularity. It should be mentioned that equilibrium points correspond to periodic regime(s) at long enough τ_1 time scale

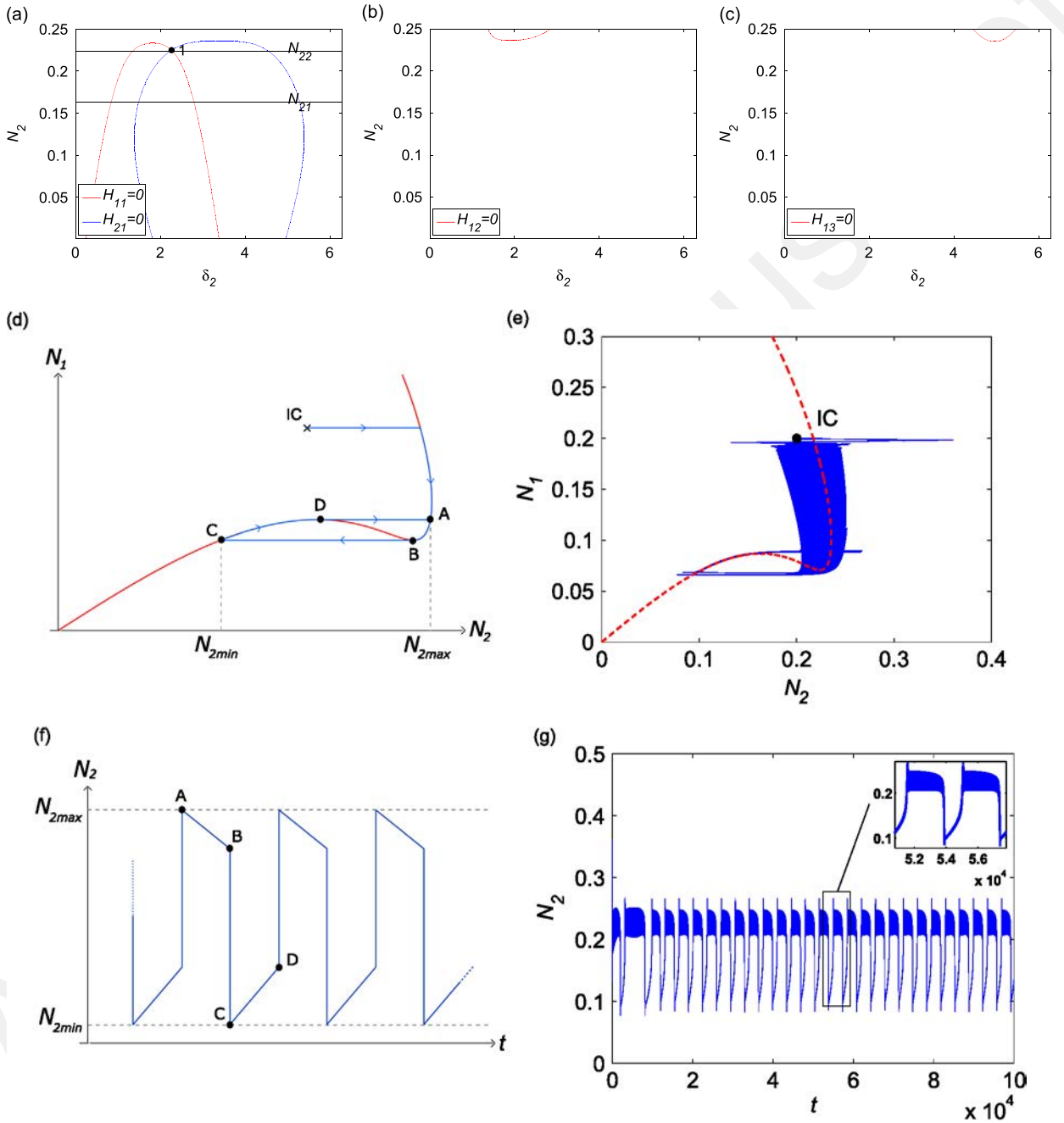

Fig. 4. *Scenario* 1 – $\mathcal{A} = 2$, $\mathcal{B} = 0.75$, $\omega_0 = 0.4$ and $f^0 = 0.105$: (a), (b), and (c) Positions of equilibrium points and fold singularities on branch ①, ② and ③ of the SIM, respectively. The system has one fold singularity on fold line N_{22} (no. 1) – (d) schematic behavior of the system during SMR in blue around the SIM: $IC \rightarrow A \rightarrow B \rightarrow C \rightarrow D$ – (e) SIM and corresponding numerical results in blue – (f) schematic evolution of the energy of the NES N_2 – (g) numerical results of the evolution of the energy of the NES N_2 – *IC* stands for "Initial Conditions". (For interpretation of the references to color in this figure caption, the reader is referred to the web version of this paper.)

while fold singularities are hints of existence of Strongly Modulated Response (SMR) [26,44]. SMR corresponds to persisting bifurcations between stable zones of the system which lead to continuous energy exchanges between the two oscillators in a quasi-periodic manner. Fig. 3 shows that the point where the tangent on the SIM becomes vertical "is not" a singular point, which means that the system will not face a direct vertical jump from branch ① to branch ③.

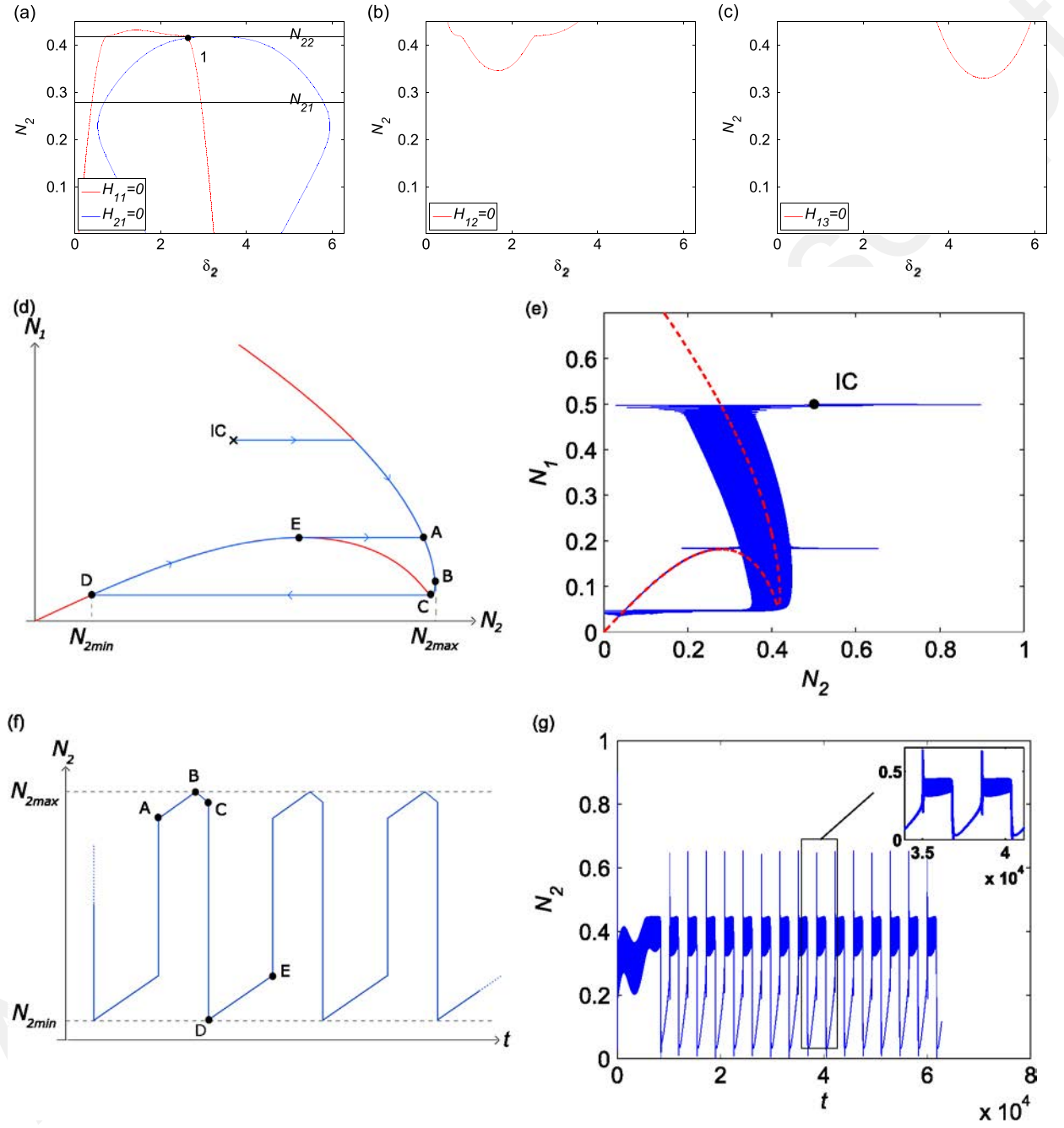

Fig. 5. *Scenario* 2 – $\mathcal{A}=2$, $\mathcal{B}=0.75$, $\omega_0=1$ and $f^0=0.32$: (a), (b), and (c) Positions of equilibrium points and fold singularities on branch ①, ② and ③ of the SIM, respectively. The system has one fold singularity on fold line N_{22} (no. 1) – (d) schematic behavior of the system during SMR in blue around the SIM: $IC \rightarrow A \rightarrow B \rightarrow C \rightarrow D \rightarrow E$ – (e) SIM and corresponding numerical results in blue – (f) schematic evolution of the energy of the NES N_2 – (g) numerical results of the evolution of the energy of the NES N_2 – *IC* stands for "Initial Conditions". (For interpretation of the references to color in this figure caption, the reader is referred to the web version of this paper.)

4.3. External forcing amplitudes leading to existence of fold singularities

Let us now exhibit the conditions of emergence of fold singularities. Introducing $\eta = re^{i\lambda}$, Eq. (32) reads:

$$\begin{cases} H_1 = \left(\beta_r - \mu_i\left(\frac{\omega_0}{2} - \mathcal{B}\rho^2\right)\right)N_2 + \frac{f^0}{2}\left(\frac{\omega_0}{2} - \mathcal{B}\rho^2\right)r\ \cos\left(\lambda - \delta_2\right) = 0 \\ H_2 = \left(\beta_i + (1+\mu_r)\left(\frac{\omega_0}{2} - \mathcal{B}\rho^2\right)\right)N_2 + \frac{f^0}{2}\left(\frac{\omega_0}{2} - \mathcal{B}\rho^2\right)r\ \sin\left(\lambda - \delta_2\right) = 0 \end{cases} \tag{37}$$

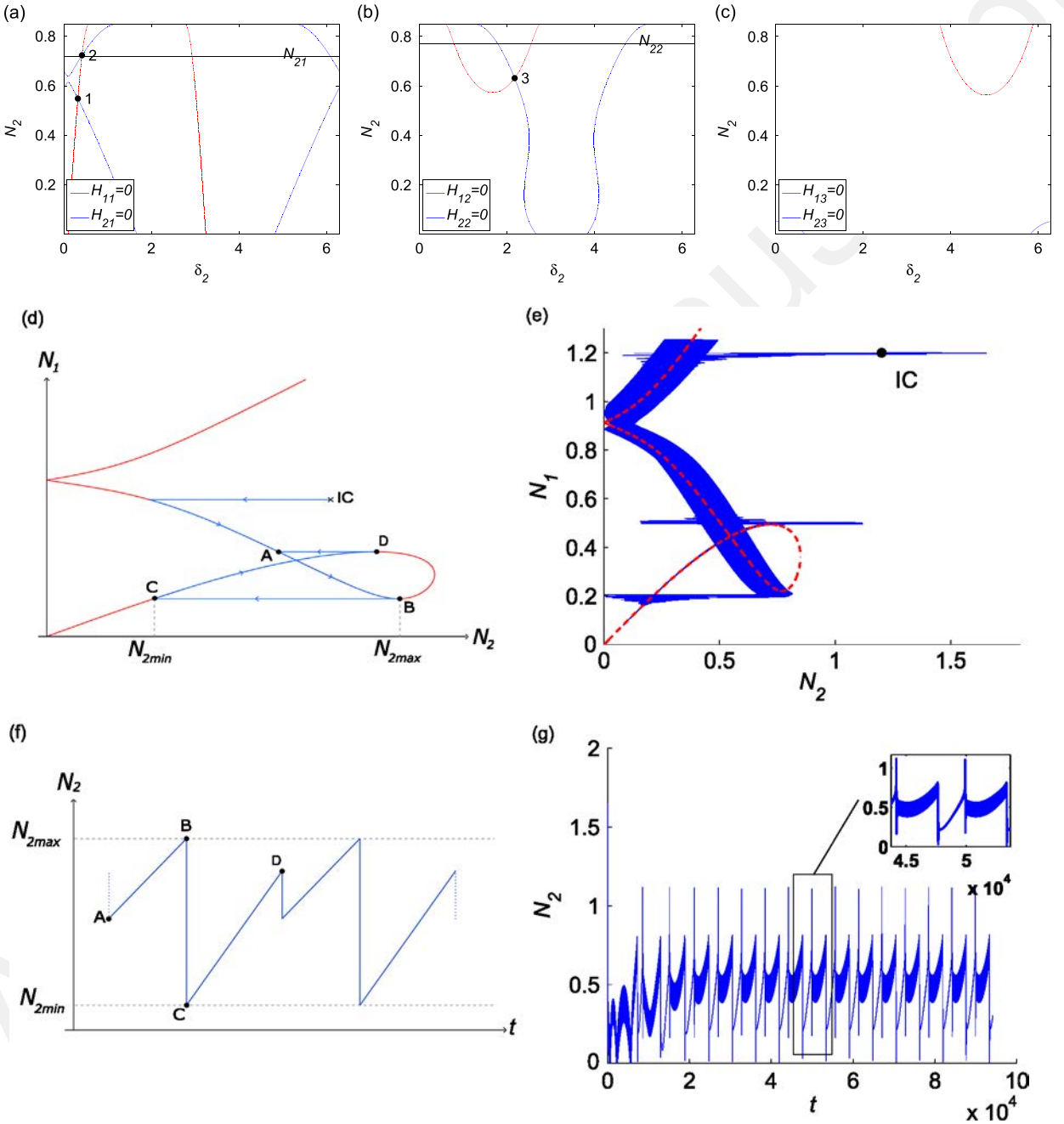

Fig. 6. *Scenario* 3 – $\mathcal{A} = 0.25$, $\mathcal{B} = 0.6$, $\omega_0 = 1$ and $f^0 = 0.81$: (a), (b), and (c) Positions of equilibrium points and fold singularities on branch ①, ② and ③ of the SIM, respectively. The system has two equilibrium points (no. 1 and no. 3) and one fold singularity on fold line N_{21} (no. 2) – (d) schematic behavior of the system during SMR in blue around the SIM: $IC \rightarrow A \rightarrow B \rightarrow C \rightarrow D$ – (e) SIM and corresponding numerical results in blue – (f) schematic evolution of the energy of the NES N_2 – (g) numerical results of the evolution of the energy of the NES N_2 – *IC* stands for "Initial Conditions". (For interpretation of the references to color in this figure caption, the reader is referred to the web version of this paper.)

One can then obtain:

$$h\left(N_2, f^0\right) = \frac{{f^0}^2}{4} r^2 \left(\frac{\omega_0}{2} - \mathcal{B}\rho^2\right)^2 - N_2^2 \left[\left(\beta_r - \mu_i\left(\frac{\omega_0}{2} - \mathcal{B}\rho^2\right)\right)^2 + \left(\beta_i + (1+\mu_r)\left(\frac{\omega_0}{2} - \mathcal{B}\rho^2\right)\right)^2\right] = 0 \tag{38}$$

Thus, forcing amplitudes leading to fold singularities, i.e. f_1^0 and f_2^0, can be obtained by solving Eq. (38) where N_2 is replaced by N_{21} and N_{22}, respectively.

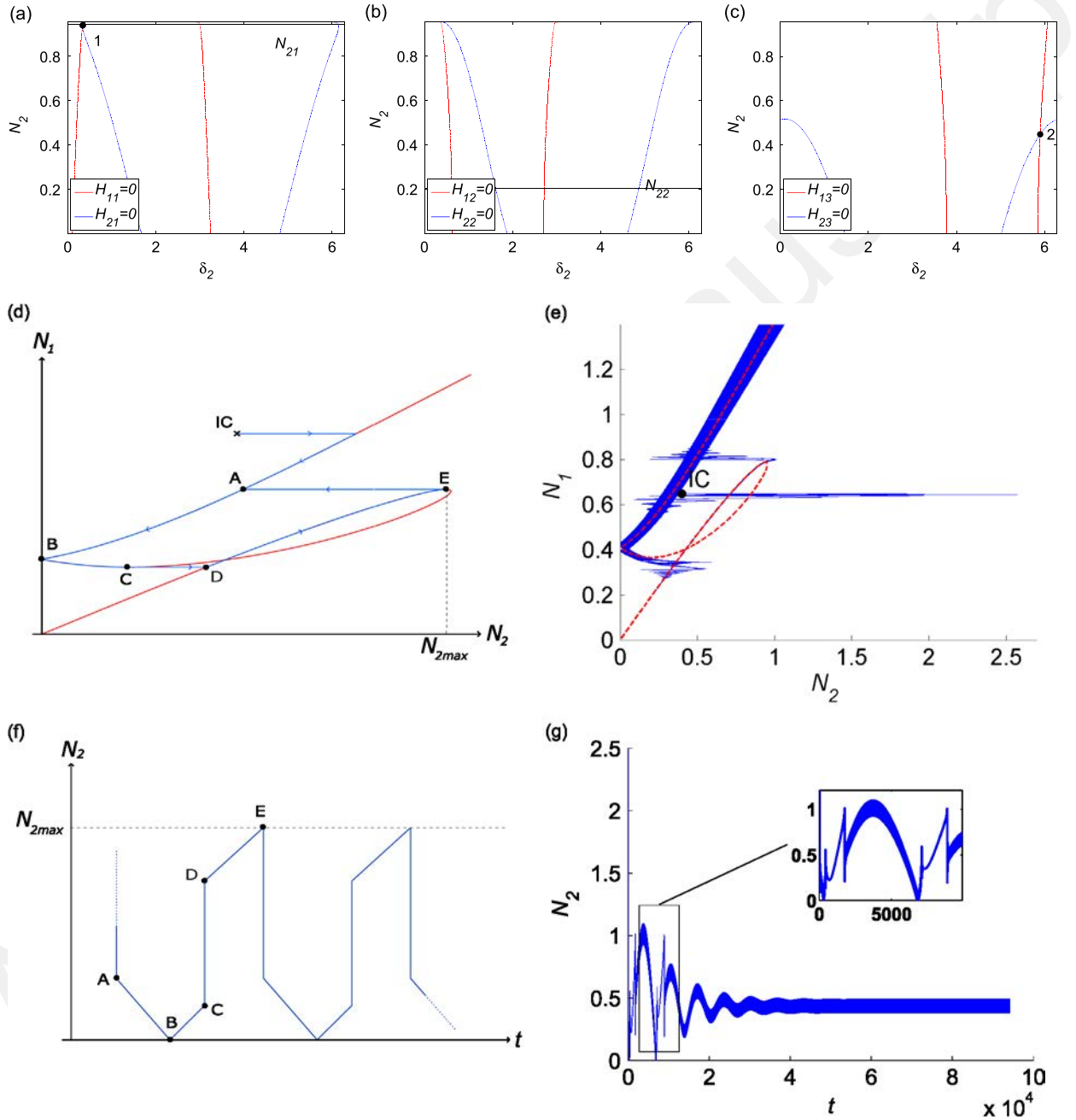

Fig. 7. *Scenario* 4 – $\mathcal{A} = 0.05$, $\mathcal{B} = 3$, $\omega_0 = 1$ and $f^0 = 1.499$: (a), (b), and (c) Positions of equilibrium points and fold singularities on branch ①, ② and ③ of the SIM, respectively. The system has one equilibrium point (no. 2) and one fold singularity on fold line N_{21} (no. 1) – (d) schematic behavior of the system during SMR in blue around the SIM: $IC \rightarrow A \rightarrow B \rightarrow C \rightarrow D \rightarrow E$ – (e) SIM and corresponding numerical results in blue – (f) schematic evolution of the energy of the NES N_2 – (g) numerical results of the evolution of the energy of the NES N_2 – *IC* stands for "Initial Conditions". (For interpretation of the references to color in this figure caption, the reader is referred to the web version of this paper.)

5. Different scenarios for SMR

Different scenarios for SMR according to the geometry of the invariant are presented in this section. Moreover, all analytical predictions are compared to numerical results.

If the system possesses fold singularities, it can present repeated bifurcations between its stable zones (between its local minimum and maximum), describing a SMR. According to the shape of the SIM, different scenarios for the geometry of the evolution of the energy of the NES can be underlined. In this section, we present five different scenarios during SMR. For each, analytical predictions are compared to numerical results obtained by direct integration of Eq. (3). The Runge–Kutta

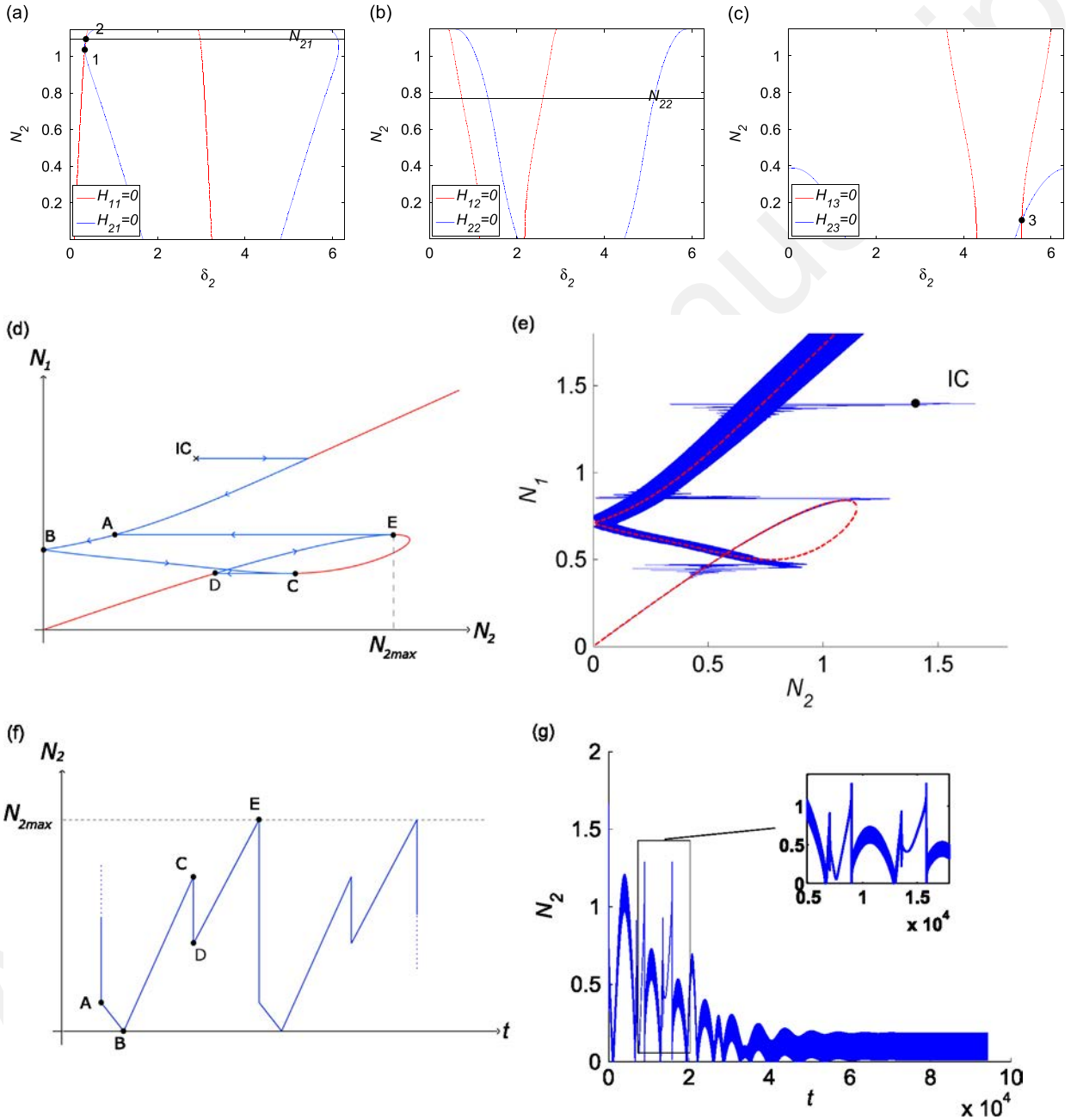

Fig. 8. *Scenario* 5 – $\mathcal{A} = 0.0667$, $\mathcal{B} = 1$, $\omega_0 = 1$ and $f^0 = 1.513$: (a), (b), and (c) Positions of equilibrium points and fold singularities on branch ①, ② and ③ of the SIM, respectively. The system has two equilibrium points (no. 1 and no. 3) and one fold singularity on fold line N_{21} (no. 2) – (d) schematic behavior of the system during SMR in blue around the SIM: $IC \rightarrow A \rightarrow B \rightarrow C \rightarrow D \rightarrow E$ – (e) SIM and corresponding numerical results in blue – (f) schematic evolution of the energy of the NES N_2 – (g) numerical results of the evolution of the energy of the NES N_2 – *IC* stands for "Initial Conditions". (For interpretation of the references to color in this figure caption, the reader is referred to the web version of this paper.)

scheme has been used thanks to the *ode45* function of Matlab. Assumed mechanical parameters are: $\epsilon = 10^{-3}$, $a_0 = 0.2$, $\Omega = 0.2$, $\sigma = 1$ and $d = 0.1$. Nonlinear stiffnesses $\mathcal{A}$ and $\mathcal{B}$, angular frequency of the main system ω_0 and external forcing amplitude f^0 will vary to describe the different scenarios. For each scenario, seven subfigures are presented. The three first subfigures (a)–(c) plot the position of equilibrium and singular points obtained from systems (35) and (36). Subfigures (d) and (f) are schematic representations of the idealized behavior of the system, i.e. the expected behavior during SMR considering only the shape of the SIM. Numerical results are also plotted: subfigure (e) compares invariant obtained from Eqs. (16) and (18)–(20) and N_1 vs N_2 obtained from direct integration of Eq. (3) while figure (g) depicts N_2 vs time also obtained from direct numerical integration. As a result, a qualitative comparison can be led between subfigures (d) and (e) and between subfigures (f) and (g), i.e. between schematic and numerical behaviors. By contrast, a quantitative comparison can be made between analytical and numerical results in subfigure (e), as well as between predicted equilibrium and singular points in subfigures (a)–(c) and system behavior in subfigures (e) and (g). Please note that fluctuations of the numerical behaviors in comparison with schematic ones may occur. It has limited consequences though, as all numerical scenarios can be differentiated and are clearly recognizable.

Let us first vary the position of the local maximum of the SIM with respect to the point where the tangent is vertical:

- *Scenario* 1: if the position of the local maximum is lower than the point with vertical tangent, the system reaches directly N_{2max} after a reverse bifurcation, then the energy decreases monotonically before a direct bifurcation from the local minimum. Fig. 4(d) and (f) depict schematically this behavior. Corresponding numerical results are obtained with $\mathcal{A} = 2$, $\mathcal{B} = 0.75$, $\omega_0 = 0.4$ and $f^0 = 0.105$. Fig. 4(a), (b) and (c) depict the position of equilibrium points and fold singularities of the system on branches ①, ② and ③, respectively. The latter possesses one fold singularity (no. 1), located on branch ①. Fig. 4(e) and (g) collects SIM, corresponding numerical results and evolutions of the energy of the NES during SMR caused by fold singularity no. 1. Assumed initial conditions are $(y(0), \dot{y}(0), x(0), \dot{x}(0)) = (0.2, 0, 0, 0)$. Shapes of envelopes during modulation are clearly connected to schematic behaviors in Fig. 4(d) and (f). Furthermore, analytical and numerical results are in good agreement in Fig. 4(e). It is the case for all four remaining scenarios.
- *Scenario* 2: if the position of the point with vertical tangent is between local maximum and minimum (see Fig. 5(d) and (e)), after a reverse bifurcation, the energy of the NES increases monotonically until it reaches N_{2max}, then it decreases monotonically before facing a direct bifurcation. Numerical simulations were obtained with $\mathcal{A} = 2$, $\mathcal{B} = 0.75$, $\omega_0 = 1$ and $f^0 = 0.32$ and initial conditions as $(y(0), \dot{y}(0), x(0), \dot{x}(0)) = (0.5, 0, 0, 0)$. The system possesses one fold singularity (no. 1), as shown in Fig. 5(a)–(c). Again, numerical results in Fig. 5(e) and (g) correspond to schematic behaviors in Fig. 5(d) and (f).

In the case where the SIM has the shape of Fig. 2(a), according to the position of the local maximum with respect to the point $\left(0, \sqrt{\frac{\omega_0}{2\mathcal{B}}}\right)$, other scenarios for the evolution of the energy N_2 can be stressed:

- *Scenario* 3: it corresponds to the case where the local maximum is below the point $\left(0, \sqrt{\frac{\omega_0}{2\mathcal{B}}}\right)$ (see Fig. 6(d) and (f)). Here, the energy of the NES increases after each bifurcation. Values of the parameter used for numerical results are $\mathcal{A} = 0.25$, $\mathcal{B} = 0.6$, $\omega_0 = 1$ and $f^0 = 0.81$ and initial conditions are $(y(0), \dot{y}(0), x(0), \dot{x}(0)) = (1.2, 0, 0, 0)$. Fig. 6(a)–(c) shows that the system has one fold singularity (no. 2) and two equilibrium points (nos. 1 and 3). Global behavior during SMR driven by fold singularity no. 2 which is collected in Fig. 6(e) and (g) is similar to the schematic one described in Fig. 6(d) and (f).
- *Scenario* 4: the position of the local maximum is higher than the point $\left(0, \sqrt{\frac{\omega_0}{2\mathcal{B}}}\right)$ and the local minimum is on the left side of the "pseudo-double point" as it is depicted in Fig. 7(d) and (f). N_2 decreases until it reaches 0 and then increases after facing a reverse bifurcation. For this scenario, following parameters were used: $\mathcal{A} = 0.05$, $\mathcal{B} = 3$, $\omega_0 = 1$, $f^0 = 1.499$, and $(y(0), \dot{y}(0), x(0), \dot{x}(0)) = (1.05, 0, 0.65, 0)$ as initial conditions. The system has one fold singularity (no. 1) and one equilibrium point (no. 2) described in Fig. 7(a)–(c). It can be seen in Fig. 7(e) and (g) that the system, after a limited couple of SMR cycles driven by fold singularity no. 1, is attracted by equilibrium point no. 2 on branch ③. The system behavior during SMR is similar to schematic behavior (see Fig. 7(d) and (f)).
- *Scenario* 5: the position of the local maximum is higher than the point $\left(0, \sqrt{\frac{\omega_0}{2\mathcal{B}}}\right)$ and the local minimum is on the right side of the "pseudo-double point", see Fig. 8(d) and (f). N_2 also decreases until it reaches 0 and increases after a reverse bifurcation, but a direct bifurcation makes N_2 decrease. Numerical simulations were obtained with $\mathcal{A} = 0.0667$, $\mathcal{B} = 1$, $\omega_0 = 1$ and $f^0 = 1.513$ and initial conditions as $(y(0), \dot{y}(0), x(0), \dot{x}(0)) = (1.4, 0, 0, 0)$. The same comments as those formulated for *Scenario* 4 can be made here about the results collected in Fig. 8(a)–(e). The system is attracted to an equilibrium point on branch ③ after two SMR cycles.

6. Conclusion

Dynamics of a two degree-of-freedom system which is composed of a main linear structure and a coupled nonlinear energy sink with local and global nonlinear potentials are studied. Global potential of the latter oscillator interacts directly with the main one while its local potential depends only on its own response. Detected slow invariant manifold of the system at fast time scale and its stable zones provide us a general view about final system behaviors. Due to the existence of the local nonlinear potential for the nonlinear energy sink, the geometry of the slow invariant manifold is different from invariants of similar systems without local potential. Indeed, the former possesses three branches instead of one, and its

three-dimensional view is necessary to interpret the system behavior. Identified equilibrium points and fold singularities of the system at slow time scale around its slow invariant manifold permit us to have finer information and more predictions about its dynamics: depending on the traced equilibrium points and fold singularities, the system can present periodic or strongly modulated responses, respectively. According to the geometry of the invariant manifold, different possible scenarios can be presented by the system during strongly modulated responses. Numerical evidence of these scenarios is qualitatively compared to idealized behaviors predicted by the shape of the slow invariant manifold. Moreover, the system behavior obtained by direct integration of system equations is in good agreement with analytical predictions as it is attracted and driven by the slow invariant manifold and its equilibrium and singular points. All developments give us tools to design nonlinear energy sinks with local potentials to be used for passive control and/or energy harvesting of main linear structural systems.

Acknowledgments

The authors would like to thank following organizations for supporting this research: (i) The “Ministère de l'Écologie, du Développement Durable et de l'Énergie” and (ii) LABEX CELYA (ANR-10-LABX-0060) of the “Université de Lyon” within the program “Investissement d'Avenir” (ANR-11-IDEX-0007) operated by the French National Research Agency (ANR).

Appendix A. Expressions of the parameters of system (32)

$$\begin{cases} \beta_r = \mathcal{R}e(\beta) = \dfrac{d}{2} \\ \beta_i = \mathcal{I}m(\beta) = -\dfrac{\Omega^2}{2\omega_0} - \mathcal{A}N_2^2 \\ \mu_r = \mathcal{R}e\left(\dfrac{\beta}{\alpha}\right) = \dfrac{a_0 d + 2\omega_0\sigma(C - 2\mathcal{A}N_2^2 - \omega_0)}{a_0^2 + 4\omega_0^2\sigma^2} \\ \mu_i = \mathcal{I}m\left(\dfrac{\beta}{\alpha}\right) = \dfrac{-2\omega_0\sigma d + a_0(C - 2\mathcal{A}N_2^2 - \omega_0)}{a_0^2 + 4\omega_0^2\sigma^2} \\ \eta_r = \mathcal{R}e\left(\dfrac{1}{\alpha}\right) = \dfrac{a_0}{\dfrac{a_0^2}{2} + 2\omega_0^2\sigma^2} \\ \eta_i = \mathcal{I}m\left(\dfrac{1}{\alpha}\right) = -\dfrac{\omega_0\sigma}{\dfrac{a_0^2}{4} + \omega_0^2\sigma^2} \end{cases} \tag{A.1}$$

References

[1] O.V. Gendelman, A.F. Vakakis, Transitions from localization to nonlocalization in strongly nonlinear damped oscillators, *Chaos, Solitons & Fractals* 11 (2000) 1535–1542.
[2] O.V. Gendelman, L.I. Manevitch, Reflection of short rectangular pulses in the ideal string attached to strongly nonlinear oscillator, *Chaos, Solitons & Fractals* 11 (2000) 2473–2477.
[3] M.J. Brennan, G. Gatti, The characteristics of a nonlinear vibration neutralizer, *Journal of Sound and Vibration* 331 (2012) 3158–3171.
[4] O.V. Gendelman, L.I. Manevitch, A.F. Vakakis, R. M'Closkey, Energy pumping in nonlinear mechanical oscillators: *part i-dynamics of the underlying hamiltonian systems*, *Journal of Applied Mechanics* 68 (2001) 34–41.
[5] A.F. Vakakis, O.V. Gendelman, Energy pumping in nonlinear mechanical oscillators: *part ii-resonance capture*, *Journal of Applied Mechanics* 68 (2001) 42–48.
[6] N.A. Alexander, F. Schilder, Exploring the performance of a nonlinear tuned mass damper, *Journal of Sound and Vibration* 319 (2008) 445–462.
[7] G. Gatti, M.J. Brennan, On the effects of system parameters on the response of a harmonically excited system consisting of weakly coupled nonlinear and linear oscillators, *Journal of Sound and Vibration* 330 (2011) 4538–4550.
[8] T. Detroux, G. Habib, L. Masset, G. Kerschen, Performance, robustness and sensitivity analysis of the nonlinear tuned vibration absorber, *Mechanical Systems and Signal Processing* 60–61 (2015) 799–809.
[9] D. McFarland, G. Kerschen, J.J. Kowtko, Y. Lee, L. Bergman, A.F. Vakakis, Experimental investigation of targeted energy transfers in strongly and nonlinearly coupled oscillators, *The Journal of the Acoustical Society of America* 118 (2005) 791–799.
[10] G. Kerschen, J.J. Kowtko, D. McFarland, Y.S. Lee, L. Bergman, A.F. Vakakis, Experimental demonstration of transient resonance capture in a system of two coupled oscillators with essential stiffness nonlinearity, *Journal of Sound and Vibration* 299 (2007) 822–838.
[11] E. Gourdon, N. Alexander, C. Taylor, C.-H. Lamarque, S. Pernot, Nonlinear energy pumping under transient forcing with strongly nonlinear coupling: theoretical and experimental results, *Journal of Sound and Vibration* 300 (2006) 522–551.
[12] B. Vaurigaud, L. Manevitch, C.-H. Lamarque, Passive control of aeroelastic instability in a long span bridge model prone to coupled flutter using targeted energy transfer, *Journal of Sound and Vibration* 330 (2011) 2580–2595.
[13] B. Vaurigaud, A. Ture Savadkoohi, C.-H. Lamarque, Targeted energy transfer with parallel nonlinear energy sinks: *part i-design theory and numerical results*, *Nonlinear Dynamics* 66 (2011) 763–780.

[14] A. Ture Savadkoohi, B. Vaurigaud, C.-H. Lamarque, S. Pernot, Targeted energy transfer with parallel nonlinear energy sinks, part ii: *theory and experiments*, *Nonlinear Dynamics* 67 (2012) 37–46.
[15] N. Wierschem, J. Luo, M. AL-Shudeifat, S. Hubbard, R. Ott, D. Quinn, D. McFarland, B.F. Spencer, A. Vakakis, L. Bergman, Experimental testing and numerical simulation of a six-story structure incorporating two-degree-of-freedom nonlinear energy sink, *Journal of Structural Engineering* 140 (2014) 04014027.
[16] E. Gourc, G. Michon, S. Seguy, A. Berlioz, Experimental investigation and design optimization of targeted energy transfer under periodic forcing, *Journal of Vibration and Acoustics* 136 (2014) 021021.
[17] Y.S. Lee, A.F. Vakakis, L.A. Bergman, D.M. McFarland, G. Kerschen, Suppressing aeroelastic instability using broadband passive targeted energy transfers: *part i-theory*, *AIAA Journal* 45 (2007) 693–711.
[18] Y.S. Lee, G. Kerschen, D. McFarland, W.J. Hill, C. Nichkawde, T. Strganac, L. Bergman, A. Vakakis, Suppressing aeroelastic instability using broadband passive targeted energy transfers: *part 2-experiments*, *AIAA Journal* 45 (2007) 2391–2400.
[19] A. Luongo, D. Zulli, Aeroelastic instability analysis of nes-controlled systems via a mixed multiple scale/harmonic balance method, *Journal of Vibration and Control* 20 (2014) 1985–1998.
[20] B. Cochelin, P. Herzog, P.O. Mattei, Experimental evidence of energy pumping in acoustics, *Comptes Rendus Mécanique* 334 (2006) 639–644.
[21] R. Bellet, B. Cochelin, R. Côte, P.-O. Mattei, Enhancing the dynamic range of targeted energy transfer in acoustics using several nonlinear membrane absorbers, *Journal of Sound and Vibration* 331 (2012) 5657–5668.
[22] J. Shao, B. Cochelin, Theoretical and numerical study of targeted energy transfer inside an acoustic cavity by a non-linear membrane absorber, *International Journal of Non-Linear Mechanics* 64 (2014) 85–92.
[23] J. Shaw, S.W. Shaw, A.G. Haddow, On the response of the non-linear vibration absorber, *International Journal of Non-Linear Mechanics* 24 (1989) 281–293.
[24] S.J. Zhu, Y.F. Zheng, Y.M. Fu, Analysis of non-linear dynamics of a two-degree-of- freedom vibration system with non-linear damping and non-linear spring, *Journal of Sound and Vibration* 271 (2004) 15–24.
[25] O.V. Gendelman, Targeted energy transfer in systems with non-polynomial nonlinearity, *Journal of Sound and Vibration* 315 (2008) 732–745.
[26] C.-H. Lamarque, O.V. Gendelman, A. Ture Savadkoohi, E. Etcheverria, Targeted energy transfer in mechanical systems by means of non-smooth nonlinear energy sink, *Acta Mechanica* 221 (1–2) (2011) 175–200.
[27] A. Ture Savadkoohi, C.-H. Lamarque, Z. Dimitrijevic, Vibratory energy exchange between a linear and a nonsmooth system in the presence of the gravity, *Nonlinear Dynamics* 70 (2012) 1473–1483.
[28] F. Nucera, A. Vakakis, A. Bergman, G. Kerschen, Targeted energy transfers in vibro-impact oscillators for seismic mitigation, *Nonlinear Dynamics* 50 (2007) 651–677.
[29] O.V. Gendelman, Analytic treatment of a system with a vibro-impact nonlinear energy sink, *Journal of Sound and Vibration* 331 (2012) 4599–4608.
[30] E. Gourc, G. Michon, S. Seguy, A. Berlioz, Targeted energy transfer under harmonic forcing with a vibro-impact nonlinear energy sink: *analytical and experimental developments*, *Journal of Vibration and Acoustics* 137 (2015) 031008.
[31] O.V. Gendelman, A. Alloni, Dynamics of forced system with vibro-impact energy sink, *Journal of Sound and Vibration* 358 (2015) 301–314.
[32] C.-H. Lamarque, A. Ture Savadkoohi, Z. Dimitrijevic, Dynamics of a linear system with time-dependent mass and a coupled light mass with non-smooth potential, *Meccanica* 49 (2014) 135–145.
[33] C.-H. Lamarque, A. Ture Savadkoohi, E. Etcheverria, Z. Dimitrijevic, Multi-scales dynamics of two coupled nonsmooth systems, *International Journal of Bifurcation and Chaos* 22 (2012) 1250295.
[34] A. Ture Savadkoohi, C.-H. Lamarque, Dynamics of coupled Dahl type and non-smooth systems at different scales of time, *International Journal of Bifurcation and Chaos* 23 (2013) 1350114.
[35] M. Weiss, A. Ture Savadkoohi, O.V. Gendelman, C.-H. Lamarque, Dynamical behavior of a mechanical system including saint-venant component coupled to a nonlinear energy sink, *International Journal of Non-Linear Mechanics* 63 (2014) 10–18.
[36] F. Schmidt, C.-H. Lamarque, Energy pumping for mechanical systems involving non-smooth saint-venant terms, *International Journal of Non-Linear Mechanics* 45 (2010) 866–875.
[37] M. Weiss, M. Chenia, A. Ture Savadkoohi, C.-H. Lamarque, B. Vaurigaud, A. Hammouda, Multi-scale energy exchanges between an elasto-plastic oscillator and a light nonsmooth system with external pre-stress, *Nonlinear Dynamics* (2015) 1–27, http://dx.doi.org/10.1007/s11071-015-2314-8.
[38] X. Jiang, D. McFarland, L.A. Bergman, A.F. Vakakis, Steady state passive nonlinear energy pumping in coupled oscillators: *theoretical and experimental results*, *Nonlinear Dynamics* 33 (2003) 87–102.
[39] G. Kerschen, A.F. Vakakis, Y.S. Lee, D.M. McFarland, J.J. Kowtko, L.A. Bergman, Energy transfers in a system of two coupled oscillators with essential nonlinearity: *1:1 resonance manifold and transient bridging orbits*, *Nonlinear Dynamics* 42 (2005) 283–303.
[40] P. Malatkar, A.H. Nayfeh, Steady-state dynamics of a linear structure weakly coupled to an essentially nonlinear oscillator, *Nonlinear Dynamics* 47 (2007) 167–179.
[41] T.L. Hill, A. Cammarano, S.A. Neild, D.J. Wagg, Interpreting the forced responses of a two-degree-of-freedom nonlinear oscillator using backbone curves, *Journal of Sound and Vibration* 349 (2015) 276–288.
[42] L.I. Manevitch, The description of localized normal modes in a chain of nonlinear coupled oscillators using complex variables, *Nonlinear Dynamics* 25 (2001) 95–109.
[43] A. Nayfeh, D. Mook, *Nonlinear Oscillations*, John Wiley and Sons, New York, 1979.
[44] Y. Starosvetsky, O.V. Gendelman, Strongly modulated response in forced 2dof oscillatory system with essential mass and potential asymmetry, *Physica D* 324 (2008) 916–939.